



Practical thermal performance correlations for molecular sieve and silica gel loaded enthalpy wheels

Jae-Weon Jeong *, Stanley A. Mumma

Department of Architectural Engineering, The Pennsylvania State University, University Park, PA 16802, USA

Received 31 March 2004; accepted 21 July 2004

Available online 21 September 2004

Abstract

The central thrust of this research was to develop practical enthalpy wheel effectiveness correlations useful for enthalpy wheel integrated systems design and analysis. In this research, enthalpy wheel performance data generated using established fundamental enthalpy wheel models were statistically analyzed. And then, first order linear regression equations were derived to estimate the enthalpy wheel sensible and latent effectiveness at normal operating rotational speeds (i.e. over 20 rpm). The two most common desiccant materials, silica gel and molecular sieve on aluminum substrate, were analyzed. Each correlation relates the enthalpy wheel sensible and latent effectiveness as a function of six parameters; incoming outdoor air and exhaust air temperature and relative humidity, face velocity, and air flow ratio. The enthalpy wheel leaving air conditions can then be simply estimated by employing the practical effectiveness correlations. Predicted effectiveness values corresponded well with published manufacturer's data and existing fundamental enthalpy wheel models.

© 2004 Elsevier Ltd. All rights reserved.

Keywords: Enthalpy wheel; Desiccant cooling; Dedicated outdoor air system; Molecular sieve; Silica gel

* Corresponding author. Tel.: +1 814 683 8313; fax: +1 814 863 4789.

E-mail address: jqj102@psu.edu (J.-W. Jeong).

Nomenclature

A	cross-sectional area of one flute, m^2
A_s	heat and mass transfer surface area on the supply or exhaust side, m^2
A'_s	heat and mass transfer surface area of one flute, m^2
C	constant describing the sorption curve shape
C^*	ratio of heat capacity rate of the air streams
C_p	specific heat, J/kg K
Cr_o^*	overall matrix heat capacity ratio
Crm_o^*	overall matrix moisture capacity ratio
D_h	hydraulic diameter of a flute, m
h	enthalpy, J/kg
h_c	convective heat transfer coefficient, $W/m^2 K$
h_{fg}	heat of vaporization, J/kg
h_m	mass transfer coefficient, m/s
k	thermal conductivity, $W/m K$
L	length of the enthalpy wheel, m
M	total mass, kg
m	mass flow rate of dry air, kg/s
m'	rate of phase change per unit length, kg/s m
N	wheel rotating speed, cycles/s
NTU_o	overall number of transfer unit
Q	air flow rate, L/s
Q_R	air flow ratio, Q_{ea}/Q_{oa}
T	temperature, $^{\circ}C$
t	time, s
U	mean air velocity in the flute, m/s
u	mass fraction of water in the desiccant
V_{fi}	face velocity, m/s
W	humidity ratio, g_w/kg_{da}
W_m	empirical coefficient describing the maximum moisture content of the desiccant, kg/kg
x	axial coordinate, m

Greek symbols

α	thermal diffusivity, m^2/s
ε	effectiveness
ϕ	relative humidity, %
η	fraction of the phase change energy delivered directly to the air
ρ	density, kg/m^3

Subscripts

a	air
---	-----

ave	averaged
d	desiccant
dry	properties at dry condition
e	exhaust side
ea	exhaust air
ei	incoming exhaust air
eq	equivalent
g	total gas phase (air and water vapor)
i	inlet
l	latent
m	matrix (including desiccant, moisture, and wheel substrate)
max	maximum
min	minimum
mt	dimensionless moisture transfer group
o	outlet
oa	outdoor air
s	sensible, supply side
sa	supply air
si	incoming supply air
t	total
v	water vapor
w	liquid water

1. Introduction

With the growing application of dedicated outdoor air systems (DOAS), a key component of which is an enthalpy wheel (also known as total energy recovery or passive desiccant wheel), practicing engineers require generally unavailable practical engineering analytical tools. The DOAS [1] supplies 100% outdoor air to each conditioned space at a rate necessary, for the most part, to meet the minimum ventilation requirements of ASHRAE Standard 62-2001 [2]. By preconditioning the incoming ventilation air with an enthalpy wheel, the DOAS heating/humidification and cooling/dehumidification energy demand and consumption operating cost savings are realized. In addition, by substantially reducing the peak design cooling and heating loads, enthalpy wheels reduce the size of HVAC equipment and associated first costs. Consequently, enthalpy wheel integrated systems provide significant sustainable and LEED [3] benefits, including high energy efficiency, reduced electric energy requirements, and reduced CFCs/HCFCs refrigerants. Moreover, DOAS systems designed to decouple the space sensible and latent loads result in better indoor air quality and thermal comfort than conventional VAV systems.

Enthalpy wheels with the familiar honeycomb matrix were introduced in US in the mid 1960s. The medium was asbestos paper impregnated with lithium chloride (LiCl). However, because of inherent absorption properties of asbestos and LiCl, these rotors had short lives. Because of environmental concerns, Kraft paper replaced asbestos paper as the matrix in the late 1970s.

In the mid 1970s, two new enthalpy wheel designs were introduced; one an oxidized aluminum wheel and the other is a silica gel wheel on an aluminum matrix. Oxidized aluminum wheels are made of corrugated aluminum foil wound on a mandrel. By dipping this assembly into a bromide solution, a layer of oxidized aluminum, a known desiccant, is formed. However, they are weak structurally and suffer from desiccant migration problems. The other enthalpy wheel design introduced in the 1970s uses silica gel bonded to an aluminum matrix substrate. This enthalpy wheel is still widely used.

From the 1980s, considerable advances have been being made in the fabrication of silica and other compounds for the semiconductor industry. A derivative of these innovations was the development of molecular sieves—synthetic zeolite desiccants that could be designed at the molecular level. At the same time, manufacturing processes developed permitting the bonding of a breathable layer of desiccant to metal or plastic surfaces. These technologies made molecular sieve enthalpy wheels, currently a very common type, possible.

While the energy and economical benefits of enthalpy wheels in HVAC applications has been known to the engineering community for some time, there have not been practical, easy to use, and reliable enthalpy wheel analytical models because of their complex characteristics of combined heat and mass transfer. The manufacturers' performance data produced in accordance with ANSI/ARI Standard 1060-2001 [4] are usually used for peak design, however off design performance analysis is currently very difficult.

To predict analytically the behavior of enthalpy wheels, the fundamental governing equations have been solved numerically [5–9]. Or alternatively the use of complicated heat and mass transfer analogies are available to predict the performance of enthalpy wheels [10–14]. Recently, some useful correlations for the sensible, latent, and total effectiveness of enthalpy wheels were proposed [15–17], however they are still complex and need many additional data.

Consequently, the main objective of this research is to provide the practicing engineering community with practical and reliable enthalpy wheel effectiveness correlations readily applicable to design and/or analysis of enthalpy wheel applications. In this research, the two enthalpy wheel designs most widely used in the industry today are considered; silica gel and molecular sieve loaded on an aluminum substrate.

The proposed enthalpy wheel correlations are developed for the normal rotating speed (i.e. over 20 rpm). In general, the enthalpy wheel operates at normal speed when the outdoor air enthalpy is higher than the relief air enthalpy; otherwise the enthalpy wheel should be off except for brief cleaning cycles. Although some manufacturers suggest modulating the enthalpy wheel speed to control the supply air temperature during the economizer and winter operation, this method of control may lead to space humidity control problems. This can occur since the sensible and latent effectiveness are quite different for most off-design wheel speeds and cannot be controlled independently via wheel speed.

2. Literature review

Before the extensive heat and mass transfer research on the relatively new enthalpy wheel or passive desiccant wheel, combined heat and mass transfer in an active desiccant wheel was well developed. In principle, the fundamental physics and surface chemistry of both passive and active

desiccant wheels are similar. However, there are a couple of major differences. Sensible heat transfer and moisture transfer are equally important in the enthalpy wheel, while sensible heat transfer is very undesirable in the active desiccant wheel. In addition, the rotational speed of the enthalpy wheel is an order of magnitude higher than that of the active desiccant wheel.

Klein et al. [7] proposed a simple ε -NTU model for silica gel enthalpy wheels rotating at infinite speed. They investigated the valid range of proposed correlations using the MOSHMX program developed by Maclaine-cross [5]. On the other hand, by curve fitting the MOSHMX calculation data for various operating conditions and matrix sizes, Stiesch et al. [18] developed the sensible and the total effectiveness correlations for molecular sieve enthalpy wheels as a function of the rotating speed. Their correlations agreed well with the manufacturer's data at relatively high rotating speed.

Simonson and Besant [19] developed a numerical model for the enthalpy wheel using the finite volume method (FVM). They considered the axial conduction, hydrodynamic and thermal entry length through the matrix, diffusion of phase change energy between the desiccant and the air, energy and moisture storage in the air, and variable heat of sorption. They also derived the fundamental dimensionless groups from governing equations, and explained the physical meaning of each dimensionless group [15].

Using these dimensionless parameters and numerical model simulation data, complex correlations for the sensible, latent, and total effectiveness of the enthalpy wheel were developed [16]. This model gives good result for a silica gel enthalpy wheel and a molecular sieve enthalpy wheel, although the uncertainty of the result increases to about $\pm 5\%$ for the molecular sieve enthalpy wheel. Simonson et al. [20] also modified this enthalpy wheel model for the unbalanced flow case (i.e. unequal SA and EA flow), while the original model is based on balanced flow.

Recently, Beccali et al. [21] proposed simple models for silica gel or LiCl enthalpy wheels. Their correlations, which predict outlet temperature and absolute humidity, were derived by interpolating the experimental data obtained from enthalpy wheel manufacturers.

On the other hand, Freund et al. [17] proposed a simple and generalized method to predict the enthalpy wheel effectiveness, which is based on the classical ε -NTU approach for the standard counter flow heat exchanger. They assumed that enthalpy wheels have characteristics similar to counter flow heat exchangers if they are operated at a sufficiently high rotation speed to eliminate effects of periodic flow. In this approach, the sensible and latent effectiveness values for a given enthalpy wheel are estimated by multiplying the Freund et al.'s correction factors by the effectiveness values of an equivalent counter flow heat exchanger. The numerical values of the Freund et al. correction factors are determined using two experimental or manufacturer's effectiveness data for the enthalpy wheel. Both balanced and unbalanced flow conditions can be considered. However, because most manufacturers only provide actual performance data at standard rating conditions recommended by ANSI/ARI Standard 1060-2001 [4], enthalpy wheel effectiveness values for non-standard rating conditions are difficult to be obtained using their model.

3. Enthalpy wheel overview

In this research, practical and reliable enthalpy wheel correlation equations for the sensible and latent effectiveness values under both balanced and unbalanced flow were developed by applying

statistical methods to performance data laboriously generated by using established fundamental models (i.e. Simonson and Besant's [16] for balanced flow and Simonson et al.'s [20] for unbalanced flows). This approach was selected over analyzing actual experimental data for various operating conditions and enthalpy wheel designs since such data are very difficult to obtain. Their model is simpler and easier to use than other numerical models, but are still complex and require information that is often difficult to obtain, such as detailed geometrical and material properties. Therefore, in this research, more practical and useful enthalpy wheel correlations are developed which can be easily used by the engineering community without as much detailed information about the enthalpy wheel.

3.1. Typical commercial enthalpy wheels

By reviewing several “leading” enthalpy wheel manufacturers' catalog data, it was found that the majority of commercial enthalpy wheels are made up of silica gel or 3–4 Å molecular sieve desiccants loaded onto a honeycomb type aluminum matrix (Fig. 1). Thin (e.g. 0.07 mm thickness) aluminum foil is corrugated to make tiny (e.g. 1.5 mm tall by 3 mm wide) sinusoidal flutes of the matrix. Desiccants account for about 20% of total enthalpy wheel mass, meaning the bulk of the sensible heat transfer is accomplished by the aluminum matrix. There are various enthalpy wheel diameter options (e.g. 0.5–5 m diameter), but the standard wheel depth of 0.2 m is nearly universal. Non-metallic materials such as paper, plastic, synthetic fiber, or glass fiber are also used for the enthalpy wheel matrix. However, these materials are more widely used for active desiccant wheels where sensible heat transfer is not desirable.

3.2. Desiccant materials

How well an enthalpy wheel performs is strongly dependent upon the desiccant chosen. Silica gel is one of the most commonly used desiccants. It can absorb water up to 40% of its own weight and withstand relatively high acidic environments. Because of good water vapor adsorption characteristic, or sorption isotherm, over a wide range of relative humidity, silica gel has generally

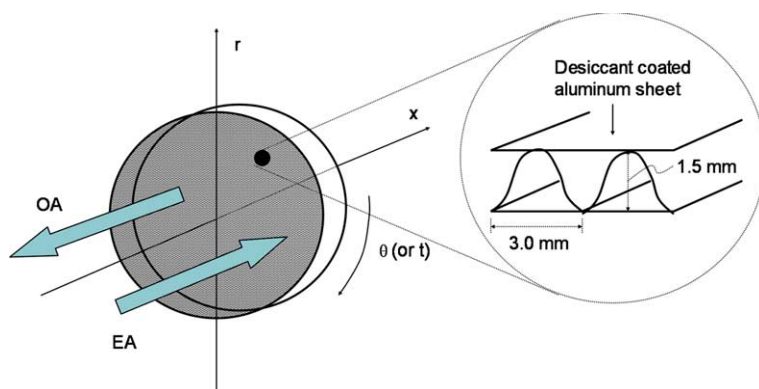


Fig. 1. Typical enthalpy wheel geometry.

been the first-choice. In addition, it has no known toxic properties. However, the decrease in adsorption capacity of silica gel with increasing temperature is significant compared to a molecular sieve. Moreover, strong alkalis (e.g. ammonia) may harm the silica gel.

Molecular sieves have a high sorption capacity at low water vapor concentrations, and maintain the high sorption capacity at elevated relative humidity. Its equilibrium water capacity is up to 20% by weight. Molecular sieves have no known toxic properties, but exposure to air that contains high concentrations of strong acids may harm them. The decrease in adsorption capacity of molecular sieve with increasing of temperature is much smaller than that of silica gel.

On the other hand, the selective adsorption characteristic of molecular sieves can mitigate the indirect cross contamination problem. According to literature [22], 3 Å molecular sieves can provide excellent selective adsorption characteristic to water vapor (2.8 Å) by excluding the adsorption of contaminant molecules that have a diameter greater than 3 Å. Other desiccants, such as silica gel, oxidized aluminum, and 4 Å molecular sieves do not provide the selective adsorption characteristic for water vapor.

3.3. Purge section

As the enthalpy wheel rotates from the exhaust air stream into the supply air stream, a small volume of the exhaust air is traversing the flutes of the wheel matrix as it passes by the seal separating the two air streams. If this volume of exhaust air were allowed to mix with the clean supply air, cross contamination would occur. In practice, this direct cross contamination can be virtually eliminated by a purge section which is an integral part of the casing design. The purge section utilizes the pressure difference which exists between the outdoor and return air streams to purge the matrix with clean outdoor air prior to its rotation into the supply air stream. Since neither thorough published experimental nor theoretical research on purge section effects are common, it has been assumed in most theoretical heat and mass transfer researches that the purge flow effect on enthalpy effectiveness is small because of its relatively small flow quantity. For many applications, cross contamination is not much of an issue since common VAV systems recirculate up to 80% of the building air.

3.4. Heat and mass transfer in enthalpy wheels

The governing equations for coupled heat and moisture transfer in enthalpy wheels are usually derived based upon the following assumptions; (1) the heat and mass transfer can be modeled using the bulk mean temperature and moisture concentrations of the air within each flute shown in Fig. 1. (2) The axial (x direction) heat conduction and water vapor molecular diffusion in the air are negligible. (3) The axial molecular diffusion and capillary motion of moisture within desiccants are negligible. (4) No radial (r direction) temperature or moisture gradients in the matrix. (5) The heat conduction through the matrix in the axial direction is dominated by the conduction through the aluminum substrate. (6) The half-plane and ends of each matrix flute are impermeable and adiabatic. (7) The air flow in the flute is fully developed laminar flow. (8) The flutes are identical with constant heat and mass transfer surface areas. (9) The matrix thermal and moisture properties are constant. Based on these assumptions, energy and mass balance equations for the air and matrix can be written for one flute.

- Energy equation for the air

$$(\rho C_p A)_g \frac{\partial T_g}{\partial t} + U(\rho C_p A)_g \frac{\partial T_g}{\partial x} - \underset{\text{(phase change)}}{m' h_{fg} \eta} + h_c \frac{A'_s}{L} (T_g - T_m) = 0 \quad (1)$$

- Energy equation for the matrix

$$(\rho C_p A)_m \frac{\partial T_m}{\partial t} - \underset{\text{(phase change)}}{m' h_{fg} (1 - \eta)} - \underset{\text{(phase change)}}{m' C_{pw} (T_g - T_m)} - h_c \frac{A'_s}{L} (T_g - T_m) = \frac{\partial}{\partial x} \left(kA \frac{\partial T}{\partial x} \right)_m \quad (2)$$

- Conservation of mass for the water vapor

$$A_g \frac{\partial \rho_v}{\partial t} + \frac{\partial}{\partial x} (\rho_v U A_g) + \underset{\text{(phase change)}}{m'} = 0 \quad (3)$$

- Conservation of mass for the dry air

$$\frac{\partial \rho_a}{\partial t} + \frac{\partial}{\partial x} (\rho_a U) = 0 \quad (4)$$

- Conservation of mass for the matrix

$$m' = \rho_{d,dry} A_d \frac{\partial u}{\partial t} \quad (5)$$

In the energy equations (Eqs. (1) and (2)), the fraction of the phase change energy (η) convected directly into the air can be approximated by Eq. (6) proposed by Simonson and Besant [19]. The value of η will not be constant for all enthalpy wheels, but is expected to range between 0 and 0.1.

$$\eta = \frac{h_c D_h / \sqrt{\alpha_s}}{h_c D_h / \sqrt{\alpha_a} + k_d / \sqrt{\alpha_d}} \quad (6)$$

During adsorption and desorption, the rate of phase change (m') shown in Eqs. (1)–(3), and (5) can be calculated by Eq. (7). The mass fraction of water in the desiccant (u) in Eq. (5) is generally presented by Eq. (8).

$$m' = h_m \frac{A'_s}{L} (\rho_v - \rho_{v,m}) \quad (7)$$

$$u = \frac{W_m}{1 - C + C/\phi} \quad (8)$$

With the addition of the fundamental psychrometric relationships for moist air, the formulation of the enthalpy wheel problem is completed. For the last couple of decades, researchers have solved the above coupled heat and mass transfer equations numerically. However, those numerical formulations were so complex that they could not be widely used by the practicing engineering community. To reduce the complexity of the numerical models, Simonson and Besant [16] pro-

posed simpler correlations for the sensible, latent, and total effectiveness of the enthalpy wheel for the balanced flow (Eqs. (9)–(16)) by correlating their numerical model simulation data.

$$\varepsilon_l = \frac{NTU_o}{1 + NTU_o} \left(1 - \frac{1}{0.54(Crm_{t,o}^*)^{0.86}} \right) \cdot \left(1 - \frac{1}{(NTU_o)^{0.51} \cdot (Crm_{t,o}^*)^{0.54} \cdot H^*} \right) \quad (9)$$

$$\varepsilon_s = \frac{NTU_o}{1 + NTU_o} \left(1 - \frac{1}{7.5Cr_o^*} \right) - \frac{H^*}{C^{*0.33}} \cdot \left[\frac{0.26 \left(\frac{Cr_o^*}{W_m^2 \cdot Crm_o^*} \right)^{0.28}}{7.2(Cr_o^*)^{1.53} + \frac{210}{(NTU_o)^{2.9}} - 5.2} + \frac{0.31\eta}{(NTU_o)^{0.68}} \right] \quad (10)$$

$$\varepsilon_t = \frac{\varepsilon_s + \varepsilon_l H^*}{1 + H^*} \quad (11)$$

$$NTU_o = \frac{1}{(mC_p)_{\min}} \left[\frac{1}{(hA_s)_s} + \frac{1}{(hA_s)_e} \right]^{-1} \quad (12)$$

$$Cr_o^* = \frac{(MC_p)_m N}{(mC_p)_{\min}} \quad (13)$$

$$Crm_o^* = \frac{M_{d,dry} N}{m_{\min}} \quad (14)$$

$$Crm_{t,o}^* = (Crm_o^*)^{0.58} W_m^{0.33} \left(\frac{\partial u}{\partial \phi} \Big|_{\phi_{ave}} \right)^{0.2} (Cr_o^*)^{1.13} \left(\frac{e \left(\frac{1482}{T_{ave}} \right)}{47.9} - 1.26(\phi_{ave})^{0.5} \right)^{4.66} \quad (15)$$

$$H^* = \frac{\Delta H_1}{\Delta H_s} = \left(\frac{\Delta H_s}{\Delta H_1} \right)^{-1} - 1 = 2500 \frac{\Delta W}{\Delta T} \quad (16)$$

where, $0 \leq \eta \leq 0.1$, $-6 \leq H^* \leq 6$, $2 \leq NTU_o \leq 10$, $3 \leq Cr_o^* \leq 10$, $1 \leq \frac{Cr_o^*}{Crm_o^*} \leq 5$, $0.1 \leq W_m \leq 0.5$, and $C^* = 1$.

On the other hand, Simonson et al. [20] modified the above effectiveness correlations to handle the unbalanced flow case. They developed equivalent equations for NTU_o , Cr_o^* , and Crm_o^* (Eqs. (17)–(19)) as a function of the flow ratio C^* defined by Eq. (20). By replacing those equivalent values (i.e. $NTU_{o,eq}$, $Cr_{o,eq}^*$, and $Crm_{o,eq}^*$) with NTU_o , Cr_o^* , and Crm_o^* in the balanced flow correlations, the equivalent sensible effectiveness ($\varepsilon_{s,eq}$) and equivalent latent effectiveness ($\varepsilon_{l,eq}$) can be calculated. The sensible and latent effectiveness values for the enthalpy wheel with unbalanced flow rates are finally determined using Eq. (21).

$$NTU_{o,eq} = \frac{2NTU_o C^*}{1 + C^*} \quad (17)$$

$$Cr_{o,eq}^* = \frac{2Cr_o^*C^*}{1 + C^*} \quad (18)$$

$$Crm_{o,eq}^* = \frac{2Crm_o^*C^*}{1 + C^*} \quad (19)$$

$$C^* = \frac{m_{\min}}{m_{\max}} \quad (\text{i.e. balanced flow : } C^* = 1.0; \text{ unbalanced flow : } C^* < 1.0) \quad (20)$$

$$\varepsilon_{s(l)} = \frac{1 - \exp \left[\varepsilon_{s(l),eq} \frac{C^{*2} - 1}{2C^*(1 - \varepsilon_{s(l),eq})} \right]}{1 - C^* \exp \left[\varepsilon_{s(l),eq} \frac{C^{*2} - 1}{2C^*(1 - \varepsilon_{s(l),eq})} \right]} \quad (21)$$

An additional modification is that the average temperature (T_{ave}) and humidity (ϕ_{ave}) in Eq. (15) should be a mass flow rate-based average (Eqs. (22) and (23)) rather than a simple arithmetic average.

$$T_{ave} = \frac{m_s T_{si} + m_e T_{ei}}{m_s + m_e} \quad (22)$$

$$\phi_{ave} = \frac{m_s \phi_{si} + m_e \phi_{ei}}{m_s + m_e} \quad (23)$$

Simonson and Besant's [16,20] models are simpler than other numerical models, but have not been widely used because they are still complex and require information that is often difficult to obtain, such as detailed geometrical and material properties.

4. Derivation of practical enthalpy wheel effectiveness correlations

Once the physical geometry and key materials of enthalpy wheel construction are determined, the sensible and latent effectiveness for enthalpy wheels operating at normal rotational speeds (i.e. over 20 rpm) could be simply described as a function of incoming OA and EA conditions including; face velocity (V_{fi}), OA temperature (T_{si}) and relative humidity (ϕ_{si}), EA temperature (T_{ei}) and relative humidity (ϕ_{ei}), and EA to OA flow ratio (Q_R) (Eq. (24)).

$$E_{s(l)} = f(V_{fi}, T_{si}, T_{ei}, \phi_{si}, \phi_{ei}, Q_R) \quad (24)$$

The proposed practical enthalpy wheel effectiveness correlations are based upon a statistical analysis of the impacts of those six independent variables and their combinations using the 2^k factorial experiment design method [23]. The superscript k means the total number of variables considered in an experiment or simulation. For each variable, only two values (i.e. high and low values) are generally considered.

The 2^k factorial experiment design method is frequently applied to design physical experiments. It is typical to repeat each experiment several times (so called replication), and to compute effects of each considering variables on the response variable using the average response. And then estimating the error associated with the measurement of each response variable and the probability that differences in average responses would have occurred due to experimental error. However,

Table 1
High and low values for the six independent variables

Label	Parameter	Low	High
A	Face velocity (V_{si}), m/s	1.0	5.0
B	OA temperature (T_{si}), °C	0	40
C	EA temperature (T_{ei}), °C	20	26
D	OA relative humidity (ϕ_{si}), %	20	80
E	EA relative humidity (ϕ_{ei}), %	30	60
F	EA to OA flow ratio ($Q_R = Q_{ea}/Q_{oa}$)	0.5	1.0

when the 2^k factorial experimental design method is applied to analyze simulation results, the replication process is not required. In addition, computer simulations are not subject to randomized experimental error.

In Table 1, high and low values for each independent variable considered in this research are presented. In this particular case, 2^6 (=64) experiments must be performed for the full factorial experiment since there are six variables to consider. The practical enthalpy wheel effectiveness correlations derived in the following sections are valid over the entire ranges for the variables listed in Table 1. When the proposed correlations are used outside of the ranges, caution should be exercised.

4.1. Practical correlations for silica gel enthalpy wheel

By analyzing silica gel enthalpy wheel performance data obtained by 2^6 simulations, single parameters and their interactions which have significant effects on the maximum sensible and latent effectiveness values were identified. Table 2 shows the percent contribution of each selected

Table 2
Percent contribution of selected parameters in silica gel enthalpy wheel

<i>Sensible effectiveness (ϵ_s)</i>						
Parameter	V_{si}	T_{si}	ϕ_{si}	Q_R	$V_{si} \cdot T_{si}$	$V_{si} \cdot \phi_{si}$
Contribution %	85.36	0.18	0.49	8.86	0.26	0.63
Parameter	$V_{si} \cdot Q_R$	$T_{si} \cdot \phi_{si}$	$T_{si} \cdot Q_R$	$V_{si} \cdot T_{si} \cdot \phi_{si}$		
Contribution %	1.75	0.68	0.15	0.86		
<i>Latent effectiveness (ϵ_l)</i>						
Parameter	V_{si}	T_{si}	T_{ei}	ϕ_{si}	ϕ_{ei}	Q_R
Contribution %	75.06	3.86	0.34	0.13	0.46	2.97
Parameter	$V_{si} \cdot T_{si}$	$V_{si} \cdot T_{ei}$	$V_{si} \cdot \phi_{si}$	$V_{si} \cdot \phi_{ei}$	$V_{si} \cdot Q_R$	$T_{si} \cdot T_{ei}$
Contribution %	3.49	0.29	0.48	0.46	0.26	0.94
Parameter	$T_{si} \cdot \phi_{si}$	$T_{si} \cdot \phi_{ei}$	$T_{si} \cdot Q_R$	$T_{ei} \cdot \phi_{si}$	$T_{ei} \cdot \phi_{ei}$	$\phi_{si} \cdot \phi_{ei}$
Contribution %	0.72	1.59	0.64	0.29	0.31	0.68
Parameter	$V_{si} \cdot T_{si} \cdot T_{ei}$	$V_{si} \cdot T_{si} \cdot \phi_{si}$	$V_{si} \cdot T_{si} \cdot \phi_{ei}$	$V_{si} \cdot T_{si} \cdot Q_R$	$V_{si} \cdot T_{ei} \cdot \phi_{ei}$	$V_{si} \cdot \phi_{si} \cdot \phi_{ei}$
Contribution %	0.60	0.43	1.25	0.81	0.31	0.53
Parameter	$T_{si} \cdot T_{ei} \cdot \phi_{si}$	$T_{si} \cdot T_{ei} \cdot \phi_{ei}$	$T_{si} \cdot \phi_{si} \cdot \phi_{ei}$	$T_{ei} \cdot \phi_{si} \cdot \phi_{ei}$	$T_{si} \cdot T_{ei} \cdot \phi_{si} \cdot \phi_{ei}$	
Contribution %	0.15	0.26	0.34	0.21	0.31	

parameter to the sensible and latent effectiveness. Formulas for computing the percent contribution can be found in the statistics text [23]. In this analysis, face velocity (V_{si}) and air flow ratio (Q_R) showed very high contribution to both sensible and latent effectiveness. On the other hand, the entering OA and EA conditions (i.e. T_{si} , ϕ_{si} , T_{ei} , and ϕ_{ei}) showed relatively small contributions to sensible effectiveness, but they showed higher contribution to latent effectiveness. Other parameters which are not presented in Table 2 showed negligible contributions (<0.13%).

From the above results, two first order linear regression equations expressing the sensible (Eq. (25)) and latent effectiveness (Eq. (26)) were derived as a function of the above selected parameters and interactions. The R^2 values for these correlations are 0.98 and 0.96, respectively.

$$\begin{aligned} \varepsilon_s = & \alpha_0 + \alpha_1(V_{si}) + \alpha_2(T_{si}) + \alpha_3(\phi_{si}) + \alpha_4(Q_R) + \alpha_5(V_{si} \cdot T_{si}) + \alpha_6(V_{si} \cdot \phi_{si}) + \alpha_7(V_{si} \cdot Q_R) \\ & + \alpha_8(T_{si} \cdot \phi_{si}) + \alpha_9(T_{si} \cdot Q_R) + \alpha_{10}(V_{si} \cdot T_{si} \cdot \phi_{si}) \end{aligned} \quad (25)$$

where,

α_0	α_1	α_2	α_3	α_4	α_5
1.06911	-0.025203	-1.02031E-003	-2.50000E-003	-0.055313	3.78125E-004
α_6	α_7	α_8	α_9	α_{10}	
2.50000E-003	-0.026562	1.10937E-003	7.81250E-004	-9.21875E-004	

$$\begin{aligned} \varepsilon_l = & \beta_0 + \beta_1(V_{si}) + \beta_2(T_{si}) + \beta_3(T_{ei}) + \beta_4(\phi_{si}) + \beta_5(\phi_{ei}) + \beta_6(Q_R) + \beta_7(V_{si} \cdot T_{si}) + \beta_8(V_{si} \cdot T_{ei}) \\ & + \beta_9(V_{si} \cdot \phi_{si}) + \beta_{10}(V_{si} \cdot \phi_{ei}) + \beta_{11}(V_{si} \cdot Q_R) + \beta_{12}(T_{si} \cdot T_{ei}) + \beta_{13}(T_{si} \cdot \phi_{si}) \\ & + \beta_{14}(T_{si} \cdot \phi_{ei}) + \beta_{15}(T_{si} \cdot Q_R) + \beta_{16}(T_{ei} \cdot \phi_{si}) + \beta_{17}(T_{ei} \cdot \phi_{ei}) + \beta_{18}(\phi_{si} \cdot \phi_{ei}) \\ & + \beta_{19}(V_{si} \cdot T_{si} \cdot T_{ei}) + \beta_{20}(V_{si} \cdot T_{si} \cdot \phi_{si}) + \beta_{21}(V_{si} \cdot T_{si} \cdot \phi_{ei}) + \beta_{22}(V_{si} \cdot T_{si} \cdot Q_R) \\ & + \beta_{23}(V_{si} \cdot T_{ei} \cdot \phi_{ei}) + \beta_{24}(V_{si} \cdot \phi_{si} \cdot \phi_{ei}) + \beta_{25}(T_{si} \cdot T_{ei} \cdot \phi_{si}) + \beta_{26}(T_{si} \cdot T_{ei} \cdot \phi_{ei}) \\ & + \beta_{27}(T_{si} \cdot \phi_{si} \cdot \phi_{ei}) + \beta_{28}(T_{ei} \cdot \phi_{si} \cdot \phi_{ei}) + \beta_{29}(T_{si} \cdot T_{ei} \cdot \phi_{si} \cdot \phi_{ei}) \end{aligned} \quad (26)$$

where,

β_0	β_1	β_2	β_3	β_4	β_5
1.35786	-0.098552	-0.025426	-0.017619	-0.028167	-0.60658
β_6	β_7	β_8	β_9	β_{10}	β_{11}
-0.021250	1.34948E-003	5.07292E-003	-0.082500	0.16042	-0.036250
β_{12}	β_{13}	β_{14}	β_{15}	β_{16}	β_{17}
1.27542E-003	0.028169	0.064142	-1.40625E-003	8.83333E-003	0.034417
β_{18}	β_{19}	β_{20}	β_{21}	β_{22}	β_{23}
-0.043333	-8.33333E-005	8.43750E-004	-2.87500E-003	1.15625E-003	-9.58333E-003
β_{24}	β_{25}	β_{26}	β_{27}	β_{28}	β_{29}
0.15000	-1.48750E-003	-2.98333E-003	-0.076167	-0.013333	3.83333E-003

The reliability of the above regression equations can be confirmed by inspecting the normal probability plot of residuals. The residual is defined as the difference between actual data and predicted data. If the points on this plot lie reasonably close to a straight line representing normal probability distribution, one can conclude that significant effects have been taken into account.

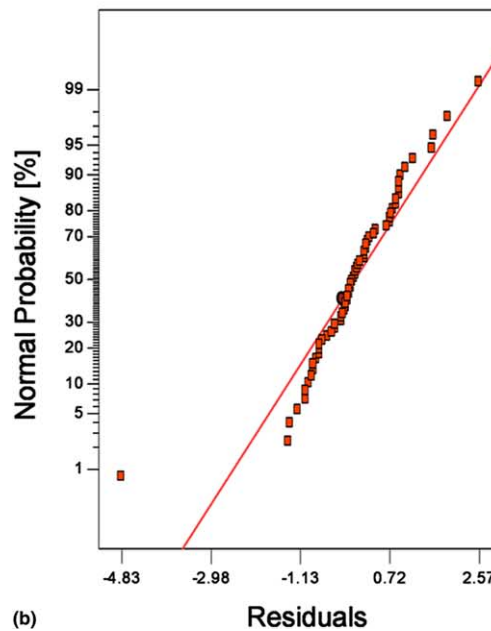
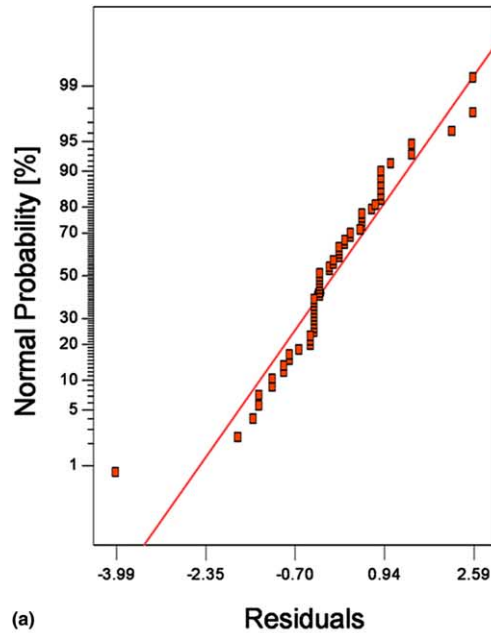


Fig. 2. Normal probability plots for (a) ε_s and (b) ε_l (silica gel enthalpy wheel).

Fig. 2 shows that normal probability plots of residuals for both sensible and latent effectiveness correlation are very close to the straight line.

4.2. Practical correlations for molecular sieve enthalpy wheel

An identical approach to that described above was used to derive practical effectiveness correlations for the molecular sieve enthalpy wheel. Table 3 shows the percent contribution of each selected parameters. Similar to the silica gel enthalpy wheel case, face velocity (V_{si}) and air flow ratio (Q_R) showed very high contribution to both sensible and latent effectiveness. The entering OA and EA conditions (i.e. T_{si} , ϕ_{si} , T_{ei} , and ϕ_{ei}) showed relatively small contributions to sensible effectiveness, but they showed higher contribution to latent effectiveness. Other parameters which are not presented in Table 3 showed negligible contributions (<0.13%).

Based on this analysis, two linear regression equations for the maximum sensible (Eq. (27)) and latent effectiveness (Eq. (28)) were derived as a function of above selected parameters and interactions. The R^2 values for these correlations are 0.98 and 0.96, respectively.

$$\begin{aligned} \varepsilon_s = & \alpha_0 + \alpha_1(V_{si}) + \alpha_2(T_{si}) + \alpha_3(\phi_{si}) + \alpha_4(Q_R) + \alpha_5(V_{si} \cdot T_{si}) + \alpha_6(V_{si} \cdot \phi_{si}) + \alpha_7(V_{si} \cdot Q_R) \\ & + \alpha_8(T_{si} \cdot \phi_{si}) + \alpha_9(T_{si} \cdot Q_R) + \alpha_{10}(\phi_{si} \cdot Q_R) + \alpha_{11}(V_{si} \cdot T_{si} \cdot \phi_{si}) + \alpha_{12}(V_{si} \cdot T_{si} \cdot Q_R) \\ & + \alpha_{13}(T_{si} \cdot \phi_{si} \cdot Q_R) \end{aligned} \quad (27)$$

Table 3
Percent contribution of selected parameters in molecular sieve enthalpy wheel

<i>Sensible effectiveness (ε_s)</i>						
Parameter	V_{si}	T_{si}	ϕ_{si}	Q_R	$V_{si} \cdot T_{si}$	$V_{si} \cdot \phi_{si}$
Contribution %	84.37	0.67	0.98	6.88	0.76	1.09
Parameter	$V_{si} \cdot Q_R$	$T_{si} \cdot \phi_{si}$	$T_{si} \cdot Q_R$	$\phi_{si} \cdot Q_R$	$V_{si} \cdot T_{si} \cdot \phi_{si}$	$V_{si} \cdot T_{si} \cdot Q_R$
Contribution %	1.16	1.22	0.22	0.13	1.35	0.17
Parameter	$T_{si} \cdot \phi_{si} \cdot Q_R$					
Contribution %	0.17					
<i>Latent effectiveness (ε_l)</i>						
Parameter	V_{si}	T_{si}	T_{ei}	ϕ_{si}	ϕ_{ei}	Q_R
Contribution %	67.34	8.33	0.59	0.13	0.81	0.36
Parameter	$V_{si} \cdot T_{si}$	$V_{si} \cdot T_{ei}$	$V_{si} \cdot \phi_{si}$	$V_{si} \cdot \phi_{ei}$	$V_{si} \cdot Q_R$	$T_{si} \cdot T_{ei}$
Contribution %	7.21	0.45	0.17	0.59	0.16	1.10
Parameter	$T_{si} \cdot \phi_{si}$	$T_{si} \cdot \phi_{ei}$	$T_{si} \cdot Q_R$	$T_{ei} \cdot \phi_{si}$	$T_{ei} \cdot \phi_{ei}$	$\phi_{si} \cdot \phi_{ei}$
Contribution %	0.13	2.11	1.18	0.17	0.40	0.67
Parameter	$V_{si} \cdot T_{si} \cdot T_{ei}$	$V_{si} \cdot T_{si} \cdot \phi_{ei}$	$V_{si} \cdot T_{si} \cdot Q_R$	$V_{si} \cdot T_{ei} \cdot \phi_{ei}$	$V_{si} \cdot \phi_{si} \cdot \phi_{ei}$	$T_{si} \cdot T_{ei} \cdot \phi_{si}$
Contribution %	0.72	1.65	1.56	0.32	0.51	0.13
Parameter	$T_{si} \cdot T_{ei} \cdot \phi_{ei}$	$T_{si} \cdot \phi_{si} \cdot \phi_{ei}$	$T_{ei} \cdot \phi_{si} \cdot \phi_{ei}$	$V_{si} \cdot T_{si} \cdot T_{ei} \cdot \phi_{ei}$	$T_{si} \cdot T_{ei} \cdot \phi_{si} \cdot \phi_{ei}$	
Contribution %	0.30	0.25	0.20	0.20	0.32	

where,

α_0	α_1	α_2	α_3	α_4	α_5
1.05319	-0.022312	1.24609E-003	5.00000E-003	-0.032000	1.17969E-004
α_6	α_7	α_8	α_9	α_{10}	α_{11}
2.50000E-003	-0.032500	-1.32813E-003	-2.32188E-003	-0.010000	-1.26562E-003
α_{12}	α_{13}				
4.53125E-004	3.62500E-003				

$$\begin{aligned} \varepsilon_1 = & \beta_0 + \beta_1(V_{si}) + \beta_2(T_{si}) + \beta_3(T_{ei}) + \beta_4(\phi_{si}) + \beta_5(\phi_{ei}) + \beta_6(Q_R) + \beta_7(V_{si} \cdot T_{si}) \\ & + \beta_8(V_{si} \cdot T_{ei}) + \beta_9(V_{si} \cdot \phi_{si}) + \beta_{10}(V_{si} \cdot \phi_{ei}) + \beta_{11}(V_{si} \cdot Q_R) + \beta_{12}(T_{si} \cdot T_{ei}) + \beta_{13}(T_{si} \cdot \phi_{si}) \\ & + \beta_{14}(T_{si} \cdot \phi_{ei}) + \beta_{15}(T_{si} \cdot Q_R) + \beta_{16}(T_{ei} \cdot \phi_{si}) + \beta_{17}(T_{ei} \cdot \phi_{ei}) + \beta_{18}(\phi_{si} \cdot \phi_{ei}) \\ & + \beta_{19}(V_{si} \cdot T_{si} \cdot T_{ei}) + \beta_{20}(V_{si} \cdot T_{si} \cdot \phi_{ei}) + \beta_{21}(V_{si} \cdot T_{si} \cdot Q_R) + \beta_{22}(V_{si} \cdot T_{ei} \cdot \phi_{ei}) \\ & + \beta_{23}(V_{si} \cdot \phi_{si} \cdot \phi_{ei}) + \beta_{24}(T_{si} \cdot T_{ei} \cdot \phi_{si}) + \beta_{25}(T_{si} \cdot T_{ei} \cdot \phi_{ei}) + \beta_{26}(T_{si} \cdot \phi_{si} \cdot \phi_{ei}) \\ & + \beta_{27}(T_{ei} \cdot \phi_{si} \cdot \phi_{ei}) + \beta_{28}(V_{si} \cdot T_{si} \cdot T_{ei} \cdot \phi_{ei}) + \beta_{29}(T_{si} \cdot T_{ei} \cdot \phi_{si} \cdot \phi_{ei}) \end{aligned} \quad (28)$$

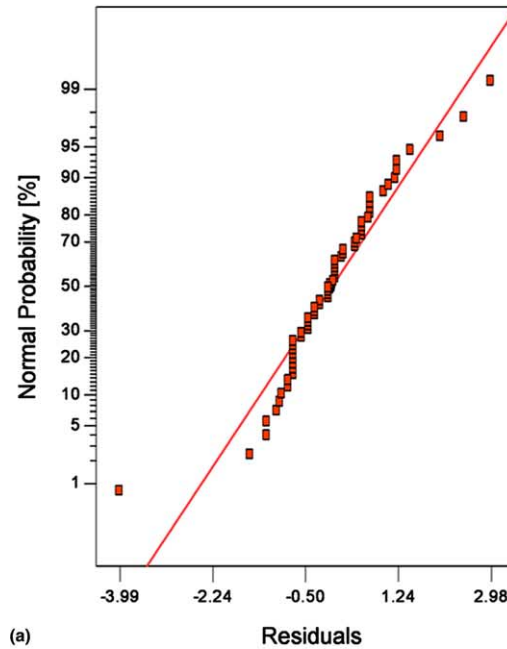
where,

β_0	β_1	β_2	β_3	β_4	β_5
1.18598	-0.026498	-0.022742	-9.82500E-003	-0.11275	-0.18408
β_6	β_7	β_8	β_9	β_{10}	β_{11}
-0.030625	-3.82031E-003	1.95833E-003	-0.11775	-0.012417	-0.031875
β_{12}	β_{13}	β_{14}	β_{15}	β_{16}	β_{17}
1.19604E-003	0.047533	0.059808	-5.96875E-003	0.014000	0.017417
β_{18}	β_{19}	β_{20}	β_{21}	β_{22}	β_{23}
0.081667	1.34375E-004	8.12500E-003	2.34375E-003	-2.91667E-003	0.21500
β_{24}	β_{25}	β_{26}	β_{27}	β_{28}	β_{29}
-2.31667E-003	-2.80417E-003	-0.11533	-0.023333	-5.62500E-004	5.66667E-003

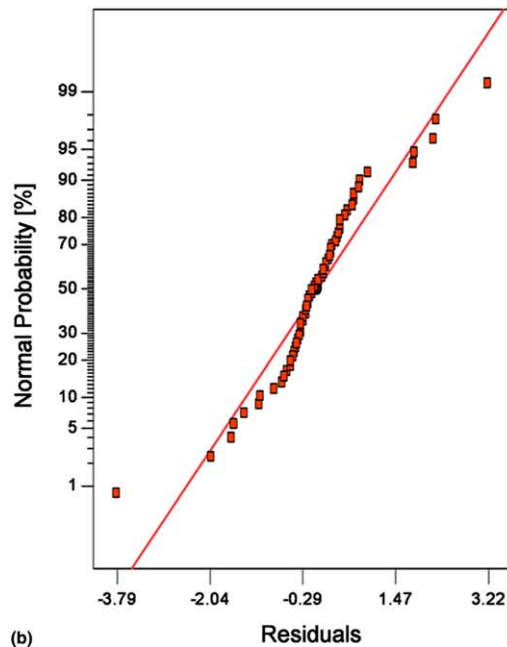
By inspecting the normal probability plot of residuals, the reliability of the proposed correlations is confirmed. Fig. 3 shows that normal probability plots of residuals for both sensible and latent effectiveness correlations are very close to the straight line which represents normal probability distribution.

4.3. Enthalpy wheel leaving air conditions

The preconditioned OA thermodynamic conditions leaving the EW, dry bulb temperature (T_{so}) and humidity ratio (W_{so}), can be computed easily with the practical correlations presented above for the sensible and latent effectiveness, Eqs. (29) and (30), respectively. The thermodynamic



(a)



(b)

Fig. 3. Normal probability plots for (a) ε_s and (b) ε_l (molecular sieve enthalpy wheel).

conditions of the relief air leaving the EW, T_{eo} and W_{eo} , can be computed in like fashion using Eqs. (31) and (32). The m_{\min} and $(mC_p)_{\min}$ are the minimum mass flow rate and the minimum capacitance flow rate, respectively, between the SA flow and the EA flow.

$$T_{so} = T_{si} - \epsilon_s \frac{(mC_p)_{\min}}{(mC_p)_s} (T_{si} - T_{ei}) \tag{29}$$

$$W_{so} = W_{si} - \epsilon_l \frac{m_{\min}}{m_s} (W_{si} - W_{ei}) \tag{30}$$

$$T_{eo} = T_{ei} + \epsilon_s \frac{(mC_p)_{\min}}{(mC_p)_e} (T_{si} - T_{ei}) \tag{31}$$

$$W_{eo} = W_{ei} + \epsilon_l \frac{m_{\min}}{m_e} (W_{si} - W_{ei}) \tag{32}$$

Once the entering and leaving air dry bulb temperature and humidity ratio conditions are known, the enthalpy values at each inlet and outlet state point can also be determined by the thermodynamic relations of moist air. Consequently, the total enthalpy effectiveness can be calculated using Eq. (33).

$$\epsilon_t = \left(\frac{m_s}{m_{\min}} \right) \left(\frac{h_{si} - h_{so}}{h_{si} - h_{ei}} \right) \tag{33}$$

Table 4
Standard rating condition (ANSI/ARI Standard 1060-2001)

Condition	Item	Entering OA (°C)	Entering EA (°C)
Summer	DBT	35	24
	WBT	26	17
Winter	DBT	1.7	21
	WBT	0.6	14

Table 5
Total effectiveness for the balanced flow (summer rating condition)

Face velocity (V_f) (m/s)	Proposed correlation (%)	Simonson and Besant (%)	Freund et al. (%)	Manufacturer's data (%)
<i>Total effectiveness (ϵ_t), $Q_R = 1.0$, silica gel EW</i>				
1.5	93.4	93.0	93.5	92.0
2.5	87.1	87.0	82.5	86.0
3.5	80.8	81.5	71.5	80.0
4.5	74.4	76.5	60.6	74.0
<i>Total effectiveness (ϵ_t), $Q_R = 1.0$, molecular sieve EW</i>				
1.5	84.9	83.5	85.5	85.0
2.5	77.2	76.0	75.5	75.5
3.5	69.4	69.5	65.5	68.0
4.5	61.7	63.5	55.4	60.0

5. Validity of the practical enthalpy wheel correlations

To verify the accuracy of the proposed practical equations, the enthalpy wheel effectiveness values predicted by the proposed correlations are compared with manufacturer's data and two exist-

Table 6
Total effectiveness for the balanced flow (winter rating condition)

Face velocity ($V_{\bar{n}}$) (m/s)	Proposed correlation (%)	Simonson and Besant (%)	Freund et al. (%)	Manufacturer's data (%)
<i>Total effectiveness (ε_t), $Q_R = 1.0$, silica gel EW</i>				
1.5	93.8	93.2	93.0	93.0
2.5	88.5	87.4	87.6	86.5
3.5	83.2	82.0	82.2	81.0
4.5	77.9	77.0	76.8	74.5
<i>Total effectiveness (ε_t), $Q_R = 1.0$, molecular sieve EW</i>				
1.5	93.3	92.8	90.4	89.0
2.5	87.5	86.0	80.4	82.5
3.5	81.6	81.0	70.5	75.0
4.5	75.8	75.0	60.0	67.0

Table 7
Effectiveness comparison for the unbalanced flow (silica gel, summer rating condition)

Face velocity ($V_{\bar{n}}$) (m/s)	Proposed correlation (%)	Simonson and Besant (%)	Freund et al. (%)
<i>Sensible effectiveness (ε_s), $Q_R = 0.8$</i>			
1.5	95.7	96.3	97.8
2.5	90.9	90.9	92.1
3.5	86.1	85.4	86.5
4.5	81.3	80.1	80.9
<i>Latent effectiveness (ε_l), $Q_R = 0.8$</i>			
1.5	94.2	96.3	97.5
2.5	87.2	90.5	89.6
3.5	80.2	84.5	81.8
4.5	73.2	78.6	73.9
<i>Sensible effectiveness (ε_s), $Q_R = 0.6$</i>			
1.5	97.1	99.1	99.9
2.5	92.8	95.4	96.9
3.5	88.5	90.2	92.1
4.5	84.3	84.6	87.3
<i>Latent effectiveness (ε_l), $Q_R = 0.6$</i>			
1.5	95.5	99.0	99.5
2.5	88.4	94.8	96.3
3.5	81.3	88.8	88.8
4.5	74.2	82.3	81.2

ing enthalpy wheel models (i.e. Simonson and Besant’s [16] and Freund et al.’s [17]). For comparison, the results have been normalized to the rating conditions of the ANSI/ARI Standard (Table 4). While the proposed practical correlations are not limited to the standard rating conditions, manufacturers’ total effectiveness and/or sensible and latent effectiveness data are only widely available for the balanced flow under the standard rating condition recommended by ASHRAE Standard 84-1991 [24] and ANSI/ARI Standard 1060-2001 [4].

5.1. Validity for the balanced flow condition

For the balanced flow, the sensible and latent effectiveness at normal rotating speed are essentially equal. Consequently, many engineers assume that the sensible, latent, and total effectiveness are identical at design rotational speed. Therefore, in this research, the total effectiveness values predicted by the proposed practical correlations, at Standard rating conditions, are compared with the total effectiveness data presented by manufacturers and that computed by published enthalpy wheel correlations.

The total effectiveness comparisons for silica gel and molecular sieve enthalpy wheels under balanced flow conditions are presented in Tables 5 and 6 at the summer and winter Standard rating conditions, respectively. The face velocity ($V_{\bar{n}}$) varies from 1.5 m/s to 4.5 m/s. As expected, the total effectiveness decreases with increasing face velocity. In addition, Tables 5 and 6 reveal that the

Table 8
Effectiveness comparison for the unbalanced flow (silica gel, winter rating condition)

Face velocity ($V_{\bar{n}}$) (m/s)	Proposed correlation (%)	Simonson and Besant (%)	Freund et al. (%)
<i>Sensible effectiveness (ϵ_s), $Q_R = 0.8$</i>			
1.5	95.6	97.7	97.8
2.5	90.3	92.7	92.1
3.5	85.1	87.4	86.5
4.5	80.0	82.3	80.9
<i>Latent effectiveness (ϵ_l), $Q_R = 0.8$</i>			
1.5	95.5	97.8	97.5
2.5	90.3	92.6	89.6
3.5	85.1	86.8	81.8
4.5	80.0	81.1	73.9
<i>Sensible effectiveness (ϵ_s), $Q_R = 0.6$</i>			
1.5	97.5	99.3	99.9
2.5	93.5	96.1	96.9
3.5	89.6	91.4	92.1
4.5	85.6	86.4	87.3
<i>Latent effectiveness (ϵ_l), $Q_R = 0.6$</i>			
1.5	97.0	99.4	99.5
2.5	92.5	96.1	96.3
3.5	88.0	90.9	88.8
4.5	83.6	85.2	81.2

effectiveness values obtained using the proposed correlations agree quite well with manufacturers' data, but there is some scatter among the various correlations.

5.2. Validity for the unbalanced flow condition

Although some manufacturers indicated that the sensible and latent effectiveness are enhanced by 2–15% under unbalanced flow condition, extensive published experimental data for unbalanced flow is very rare. Therefore, in this research, the unbalanced flow sensible and latent effectiveness values predicted by the proposed correlations are compared with the results of other enthalpy wheel correlations. Those effectiveness data are estimated for two air flow ratios (Q_R), i.e. 0.6 and 0.8 under the ANSI/ARI Standard 1060-2001 rating conditions. The face velocity (V_{fi}) varies from 1.5 m/s to 4.5 m/s.

Tables 7 and 8 present the sensible and latent effectiveness for the silica gel enthalpy wheel at standard summer and winter rating condition, respectively. Similarly, the effectiveness values for the molecular sieve enthalpy wheel are presented in Tables 9 and 10.

Manufacturers' data indicate that the sensible and latent effectiveness increases as the ratio of relief air to OA (Q_R) decreases. In other word, higher effectiveness values are obtained with unbalanced flow, but of course the energy transferred is reduced. Tables 7–10 presents comparisons of the proposed sensible and latent effectiveness correlations with other established enthalpy wheel correlations results.

Table 9
Effectiveness comparison for the unbalanced flow (molecular sieve, summer rating condition)

Face velocity (V_{fi}) (m/s)	Proposed correlation (%)	Simonson and Besant (%)	Freund et al. (%)
<i>Sensible effectiveness (ϵ_s), $Q_R = 0.8$</i>			
1.5	95.4	96.1	94.0
2.5	90.2	90.5	83.8
3.5	84.9	84.6	73.7
4.5	79.7	78.9	63.6
<i>Latent effectiveness (ϵ_l), $Q_R = 0.8$</i>			
1.5	83.4	85.0	86.1
2.5	73.4	77.6	79.2
3.5	63.5	69.9	72.3
4.5	53.5	62.2	65.4
<i>Sensible effectiveness (ϵ_s), $Q_R = 0.6$</i>			
1.5	97.0	99.0	99.9
2.5	92.1	94.9	93.3
3.5	87.2	89.1	85.7
4.5	82.3	83.1	78.2
<i>Latent effectiveness (ϵ_l), $Q_R = 0.6$</i>			
1.5	86.7	88.2	93.7
2.5	75.7	81.7	88.5
3.5	64.7	73.1	83.3
4.5	53.8	63.9	78.2

Table 10

Effectiveness comparison for the unbalanced flow (molecular sieve, winter rating condition)

Face velocity (V_f) (m/s)	Proposed correlation (%)	Simonson and Besant (%)	Freund et al. (%)
<i>Sensible effectiveness (ε_s), $Q_R = 0.8$</i>			
1.5	95.5	97.6	98.0
2.5	90.8	92.6	89.1
3.5	86.1	87.2	80.3
4.5	81.4	81.9	71.4
<i>Latent effectiveness (ε_l), $Q_R = 0.8$</i>			
1.5	93.8	97.1	90.6
2.5	87.7	90.9	84.7
3.5	81.5	83.9	78.8
4.5	75.3	77.0	72.8
<i>Sensible effectiveness (ε_s), $Q_R = 0.6$</i>			
1.5	97.3	99.3	99.9
2.5	93.2	96.0	96.3
3.5	89.1	91.1	89.7
4.5	85.0	86.0	83.0
<i>Latent effectiveness (ε_l), $Q_R = 0.6$</i>			
1.5	95.5	99.1	96.2
2.5	89.9	94.6	91.8
3.5	84.2	87.9	87.3
4.5	78.6	80.5	82.9

6. Conclusions

Practical enthalpy wheel effectiveness correlations which can be more easily used to design and analyze enthalpy wheel integrated systems were developed from published complex formulations and models using statistical methods. The proposed practical correlations are for two enthalpy wheel desiccant materials; silica gel and molecular sieve loaded onto an aluminum honeycomb matrix substrate. The correlations relate the sensible and latent effectiveness of the enthalpy wheel rotating at normal speed to the following six variables; entering OA and EA temperature and relative humidity, face velocity, and air flow ratio. The total effectiveness can also be calculated once the sensible and the latent effectiveness are estimated. From this work, it was found that the face velocity (V_{si}) and air flow ratio (Q_R) showed very high contribution to both sensible and latent effectiveness. The entering OA and EA conditions (i.e. T_{si} , ϕ_{si} , T_{ei} , and ϕ_{ei}) showed relatively small contributions to sensible effectiveness, but they showed higher contribution to latent effectiveness. The enthalpy wheel effectiveness values predicted by the proposed correlations corresponded well with the manufacturer's data and other existing enthalpy wheel model results.

Acknowledgment

Financial assistance for ASHRAE's Grant-In-Aid program is greatly appreciated.

References

- [1] S.A. Mumma, Overview of integrating dedicated outdoor air systems with parallel terminal systems, *ASHRAE Transactions* 107 (1) (2001) 545–552.
- [2] ASHRAE, ANSI/ASHRAE Standard 62-2001, Ventilation for acceptable indoor air quality, American Society of Heating, Refrigerating and Air-Conditioning Engineers, Inc., Atlanta, GA, 2001.
- [3] LEED, *Green Building Rating System for New construction & Major renovations (LEED-NG) Version 2.1*, Leadership in Energy & Environmental Design, US Green building Council, 2002.
- [4] ARI, ANSI/ARI Standard 1060-2001, Standard for Rating Air-to-Air Heat Exchangers for Energy Recovery Ventilation Equipment, Air-Conditioning and Refrigeration Institute, Arlington, VA, 2001.
- [5] I.L. Maclaine-cross, A Theory of Combined Heat and Mass Transfer in Regenerators, Ph.D. Thesis in Mechanical Engineering, Monash University, Australia, 1974.
- [6] R.K. Collier, Advanced desiccant material assessment: phase 2, Report GRI-88-0125, Chicago Gas Research Institute, 1988.
- [7] H. Klein, S.A. Klein, J.W. Mitchell, Analysis of regenerative enthalpy exchangers, *International Journal of Heat and Mass Transfer* 33 (1990) 735–744.
- [8] W. Zheng, W.M. Worek, Numerical simulation of combined heat and mass transfer processes in a rotary dehumidifier, *Numerical Heat Transfer* 23 (A) (1993) 211–232.
- [9] X.J. Zhang, Y.J. Dai, R.Z. Wang, A simulation study of heat and mass transfer in a honeycombed rotary desiccant humidifier, *Applied Thermal Engineering* 23 (2003) 989–1003.
- [10] I.L. Maclaine-cross, P.J. Banks, Coupled heat and mass transfer in regenerators—Prediction using an analogy with heat transfer, *International Journal of Heat and Mass Transfer* 15 (1972) 1225–1242.
- [11] E. Van den Bulck, J.W. Mitchell, S.A. Klein, Design theory for rotary heat and mass exchangers—I. Wave analysis of rotary heat and mass exchangers with infinite transfer coefficients, *International Journal of Heat and Mass Transfer* 28 (1985) 1575–1586.
- [12] E. Van den Bulck, J.W. Mitchell, S.A. Klein, Design theory for rotary heat and mass exchangers—II. Effectiveness-number of transfer units method for rotary heat and mass exchangers, *International Journal of Heat and Mass Transfer* 28 (1985) 1587–1595.
- [13] P.J. Banks, Prediction of heat and mass regenerator performance using nonlinear analogy method: Part 1 Basis, *ASME Journal of Heat Transfer* 107 (1985) 222–229.
- [14] P.J. Banks, Prediction of heat and mass regenerator performance using nonlinear analogy method: Part 2 Comparison of methods, *ASME Journal of Heat Transfer* 107 (1985) 230–238.
- [15] C.J. Simonson, R.W. Besant, Energy wheel effectiveness: Part I—development of dimensionless groups, *International Journal of Heat and Mass Transfer* 42 (1999) 2161–2170.
- [16] C.J. Simonson, R.W. Besant, Energy wheel effectiveness: Part II—correlations, *International Journal of Heat and Mass Transfer* 42 (1999) 2171–2185.
- [17] S. Freund, S.A. Klein, D.T. Reindl, A semi-empirical method to estimate enthalpy exchanger performance and a comparison of alternative frost control strategies, *HVAC&R Research* 9 (4) (2003) 493–508.
- [18] G. Stiesch, S.A. Klein, J.W. Mitchell, Performance of rotary heat and mass exchangers, *HVAC&R Research* 1 (4) (1995) 308–323.
- [19] C.J. Simonson, R.W. Besant, Heat and moisture transfer in desiccant coated rotary energy exchangers: Part I. Numerical model, *HVAC&R Research* 3 (4) (1997) 325–350.
- [20] C.J. Simonson, W. Shang, R.W. Besant, Part-load performance of energy wheels: Part II—Bypass control and Correlations, *ASHRAE Transactions* 106 (1) (2000) 301–310.
- [21] M. Beccali, F. Butera, R. Guarella, R.S. Adhikari, Simplified models for the performance evaluation of desiccant wheel dehumidification, *International Journal of Energy Research* 27 (2003) 17–29.
- [22] C.W. Bayer, R.J. Hendry, The importance of the desiccant in total energy wheel cross-contamination, Final report on project A-5849-000, Georgia Tech Research Institute, Atlanta, GA, 1999.
- [23] D. Montgomery, *Design and Analysis of Experiments*, 5th ed., John Wiley and Sons, 2001.
- [24] ASHRAE, ANSI/ASHRAE Standard 84-1991, Method of Testing Air-to-Air heat Exchangers, American Society of Heating, Refrigerating and Air-Conditioning Engineers, Inc., Atlanta, GA, 1991.